applied sciences

MDPI

Article

Simulation Study on the Influence of Swirl Structure on the Performance of Static Low-Concentration Coalbed Methane Mixer

Han Gao [1], Xuanping Gong [1], Sen Li [2], Qianting Hu [2] and Yongjiang Luo [2,*]

[1] Middling Coal Energy Research Institute Co., Ltd., Xi'an 710054, China; gaohan1986@126.com (H.G.); gongxuanping@chinacoal.com (X.G.)
[2] National Key Laboratory of Coal Mine Disaster Dynamics and Control, Chongqing University, Chongqing 400044, China
* Correspondence: luoyj16@cqu.edu.cn; Tel.: +86-0431-88502263; Fax: +86-0431-88502337

Abstract: The utilization of low-concentration coalbed gas as an energy source in coal mines has garnered significant attention due to the intensifying global warming trend. Achieving a uniform gas mixture is essential for the effectiveness of various gas utilization technologies. In this study, we conducted a series of numerical studies on the pressure loss and mixing uniformity of a swirl-type static low-concentration coalbed methane (SLCCM) mixer with spiral blades as turbulence elements. The results indicate that installing spiral blades at the low-concentration gas inlet can significantly improve gas mixing uniformity, while installing spiral blades at the air inlet has a relatively small impact on gas mixing uniformity. When spiral blades are installed at both the low-concentration gas and air inlets, and the spiral direction of the two sets of blades is the same, the pressure loss of the mixer is smaller than that of the mixer with opposite spiral directions. Moreover, the mixing uniformity of the former is better than that of the latter when the length of the mixing zone is shorter. However, as the length of the mixing zone increases, the mixing uniformity of the mixer with opposite spiral directions of the two sets of blades will be significantly improved and better than that of the mixer with the same spiral direction. When a set of spirals with opposite directions to the blades at the low-concentration gas inlet is added at the forefront of the mixing zone, the mixing uniformity at the outlet of the mixer can be greatly improved, but it will increase the mixing pressure loss of the system. When the two spirals are in the same direction, the impact on the system pressure loss and mixing uniformity is relatively small. The numerical simulation results show that by setting a set of spiral blades with the same rotation directions at the inlet of low-concentration gas and at the forefront of the mixing zone (i.e., b2-type structure), the spatial non-uniformity of the mixing is about 5.24%, and the system pressure loss is less than 400 Pa, which is significantly better than the requirement of less than 15% spatial non-uniformity for engineering requirements. Moreover, with the increase in the length of the mixing zone, the spatial non-uniformity still tends to decrease.

Keywords: rotational flow; static gas mixer; mixed characteristics; pressure loss

check for updates

Received: 27 February 2025
Revised: 18 April 2025
Accepted: 19 April 2025
Published: 23 April 2025

Citation: Gao, H.; Gong, X.; Li, S.; Hu, Q.; Luo, Y. Simulation Study on the Influence of Swirl Structure on the Performance of Static Low-Concentration Coalbed Methane Mixer. *Appl. Sci.* **2025**, *15*, 4676. https://doi.org/10.3390/app15094676

Copyright: © 2025 by the authors. Licensee MDPI, Basel, Switzerland. This article is an open access article distributed under the terms and conditions of the Creative Commons Attribution (CC BY) license (https://creativecommons.org/licenses/by/4.0/).

1. Introduction

According to the International Energy Agency's report "Global Methane Tracker", methane emissions from the energy sector reached nearly 130 million tons in 2023, accounting for over one-third of anthropogenic emissions, second only to the agriculture sector [1].

These emissions primarily arise from methane escaping during coal mining and unintentional emissions in the oil and gas sectors [2]. The gas escape from coal mines accounts for approximately 40% of the country's total methane emissions in China [3]. Therefore, the implementation of low-concentration gas utilization has become an important measure to reduce greenhouse gas emissions, and achieving a uniform gas mixture is essential for the effectiveness of various gas utilization technologies. In modern industrial applications, mixing is a critical process, particularly in chemical production and environmental engineering. However, traditional mixing methods struggle to achieve ideal results for high-flow-rate, high-turbulence flows and low-viscosity gases. When handling shear-insensitive gaseous media such as hydrogen or methane, mixing operations are typically conducted under turbulent flow conditions. Nevertheless, inadequate mixing in high Reynolds number turbulent states may lead to unstable flow patterns [4,5], localized concentration anomalies (excessive or insufficient), increased system energy loss, reduced reaction rates, or potential safety hazards. To address these challenges, enhancing turbulent mixing efficiency through rational structural arrangements of mixing elements while strengthening momentum and mass transfer is critically important [6].

Compared with dynamic mixers [7], static mixers have the advantages of a simple structure and no moving parts, and are suitable for continuous mixing processes. With advancements in static mixer research, particularly improvements to mixing elements, their applications have expanded from traditional solid–liquid and liquid–liquid mixing to enhanced heat transfer, gas–liquid mixing, and gas–gas mixing [8]. Compared to conventional gas mixing methods such as pipeline blending [9,10], nozzle mixing [11,12], and venturi tube mixing [13], static mixers demonstrate superior overall performance in balancing energy loss and mixing uniformity [14]. The gas mixing performance of static mixers primarily depends on the geometric shape of elements, geometric parameters, swirl positioning, rotational orientation, and structural layouts. Li et al. [15] demonstrated that dynamic mixers require additional energy input while delivering mediocre mixing efficiency and lower safety performance. Therefore, static mixers are generally preferred for blending hazardous gases like methane and natural gas. YANG Yunlan et al. [7] showed that during gas mixing, SK-type and SX-type static mixers exhibit higher turbulent kinetic energy and turbulence intensity. SK-type static mixers demonstrate maximum shear strength, while HEV-type static mixers achieve the highest shear efficiency. However, HEV-type static mixers underperform in mixing effectiveness compared to the other three types, particularly under short mixing distances (<5D). Torque-modified mixing elements prove more suitable for gas mixing processes. Existing low-concentration methane utilization systems employ static helical mixing structures [16,17], yet blending uniformity remains suboptimal. SU Yue et al. [18] utilized numerical simulations to study hydrogen–methane blending processes in follow-flow hydrogen mixing equipment with different static mixer types and operating conditions. The results indicate that turbulence-enhancing elements in mixers decisively influence blending uniformity; the proper arrangement of these elements significantly improves mixing performance [19].

Current helical mixing element configurations in static mixers lack systematic design principles [20], with existing helical mixers demonstrating unsatisfactory blending uniformity. When applied to systems like regenerative thermal oxidation, this poses risks of localized methane concentrations exceeding safe thresholds. Therefore, this study employed numerical simulations to analyze blending uniformity and pressure loss under varying helical blade configurations, providing technical support for optimizing gas blending devices.

2. SLCCM Mixer Structure Design

The performance of four different blending structures was compared, and the influence of adding spiral blades at the forefront of the mixing zone with different rotational directions on the performance of the four structures was further analyzed. Figure 1a shows a single-rotation blending structure with only air rotation, where air enters the mixing zone through internal small-diameter spiral blades to mix with gas. Figure 1b shows a single-rotation blending structure with only gas rotation, where air enters the mixing zone through external large-diameter spiral blades to mix with gas. Figure 1c shows a double-rotation blending structure with both air and gas rotating in opposite directions, where both gases enter the mixing zone through their respective spiral structures. Figure 1d shows a double-rotation blending structure with both air and gas rotating in the same direction, where both gases enter the mixing zone through their respective spiral structures. Subsequently, spiral blades with different rotational directions were added at the forefront of the mixing zone in the four different blending structures (Figure 1a–d) to further rotate and mix the two gases entering the mixing zone. The specific experimental design structural features are shown in Table 1. All spiral blades were uniformly designed with 0.5 turns, a pitch of 450 mm, and a thickness of 5 mm. The geometric parameters were fixed across all configurations to isolate the effects of swirl direction and arrangement. The adopted values were based on prior studies and are representative of effective mixing structures. Future work will involve systematic parametric studies to quantify the effects of pitch, blade geometry, and other design variables on mixing performance.

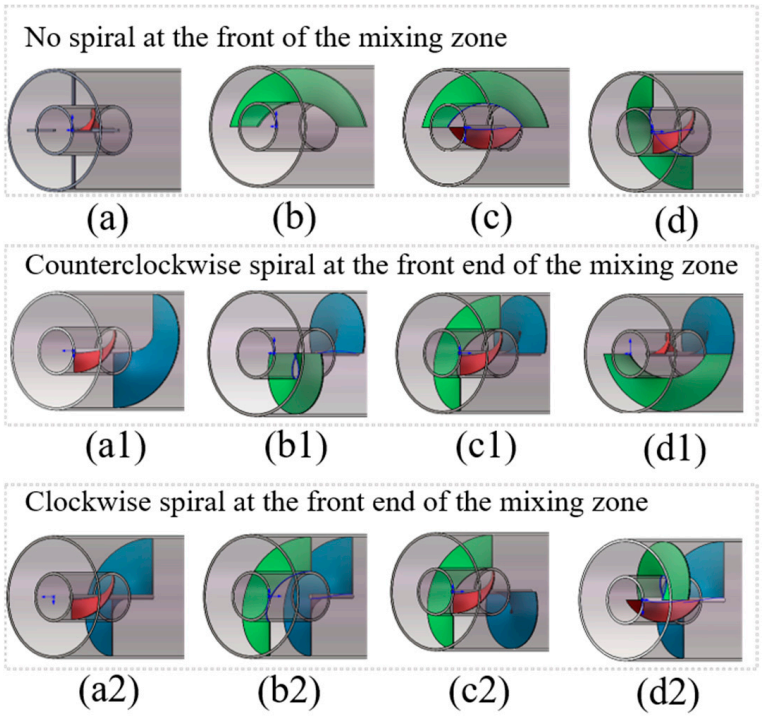


Figure 1. Four mixing structures and corresponding mixing zone screw schemes. (**a**) Air rotation, (**b**) gas rotation, (**c**) air–gas counter-rotating, (**d**) air–gas co-rotating, (**a1**) Air rotation and mixing zone front end rotate counterclockwise, (**b1**) gas rotation and mixing zone front end rotate counterclockwise, (**c1**) air–gas counter-rotating and mixing zone front end rotate counterclockwise, (**d1**) air–gas co-rotating and mixing zone front end rotate counterclockwise, (**a2**) Air rotation mixing zone front end rotate clockwise, (**b2**) gas rotation mixing zone front end rotate clockwise, (**c2**) air–gas counter-rotating mixing zone front end rotate clockwise, (**d2**) air–gas co-rotating mixing zone front end rotate clockwise.

Table 1. Experimental design structural features.

Test ID	Air Vane Helix	Rotation Dir.	Gas Vane Helix	Rotation Dir.	Helical Vane (Mixing Zone)	Rotation Dir.
a	Yes	Counterclockwise	No	No	No	No
a1	Yes	Counterclockwise	No	No	Yes	Counterclockwise
a2	Yes	Counterclockwise	No	No	Yes	Clockwise
b	No	No	Yes	Clockwise	No	No
b1	No	No	Yes	Clockwise	Yes	Counterclockwise
b2	No	No	Yes	Clockwise	Yes	Clockwise
c	Yes	Counterclockwise	Yes	Clockwise	No	No
c1	Yes	Counterclockwise	Yes	Clockwise	Yes	Counterclockwise
c2	Yes	Counterclockwise	Yes	Clockwise	Yes	Clockwise
d	Yes	Counterclockwise	Yes	Counterclockwise	No	No
d1	Yes	Counterclockwise	Yes	Counterclockwise	Yes	Counterclockwise
d2	Yes	Counterclockwise	Yes	Counterclockwise	Yes	Clockwise

3. Computational Model

The flow of gas follows the laws of mass conservation, momentum conservation, and energy conservation. The fundamental equations of fluid mechanics are the continuity equation, momentum conservation equation, and energy conservation equation. The mass conservation equation states that the increase in mass within a fluid element per unit of time is equal to the net mass flowing into the element during the same time interval. The continuity equation is as follows:

For steady flow, $\frac{\partial \rho}{\partial t} = 0$, the continuity equation is

$$\frac{\partial \rho}{\partial t} + div(\rho u) = 0 \tag{1}$$

$$div(\rho u) = 0. \tag{2}$$

For incompressible fluids, $\frac{D\rho}{Dt} = 0$, the equation is

$$divu = 0. \tag{3}$$

In the above equations, ρ is density, t is time, and u is the velocity vector.

The momentum conservation law states that the rate of change of momentum of a fluid element with respect to time is equal to the sum of the external forces acting on the element. That is

$$\rho \frac{Du}{Dt} = \rho F_b + divP \tag{4}$$

where P is the pressure on the fluid element and F_b is the body force on the element.

The basic control equations are established based on laminar flow, but the mixing process is turbulent. To ensure good simulation results, the control equations need to be modified. Generally, turbulent flow is extremely complex, and the N–S model is a relatively accurate method for numerical calculation of flow. However, due to its high computational accuracy, it requires high CPU speed and memory size, making it generally unsuitable for engineering calculations. Common turbulence simulation methods suitable for engineering calculations include Large Eddy Simulation (LES) and Reynolds-Averaged Navier–Stokes (RANS).

In this study, the standard $k - \varepsilon$ [21] model was used. Due to its computational accuracy and convergence, it meets the general requirements of engineering calculations

and is widely used in engineering. This model uses the turbulence kinetic energy equation and the turbulence dissipation rate equation to close the turbulence control equations:

$$\frac{\partial(\rho k)}{\partial t} + \nabla\bullet(\rho\vec{V}k) = \nabla\bullet(\Gamma_k\nabla k) + G_k + G_b - \rho\varepsilon - Y_k + S_k \quad (5)$$

$$\frac{\partial(\rho k)}{\partial t} + \nabla\bullet\left(\rho\vec{V}\varepsilon\right) = \nabla\bullet(\Gamma_k\nabla\varepsilon) + G_{1\varepsilon}\frac{\varepsilon}{k}(G_K + G_{3\varepsilon}G_b) - G_{2\varepsilon}\rho\frac{\varepsilon^2}{k} + S_\varepsilon \quad (6)$$

where the model constants are $C_\mu = 0.09, C_{1\varepsilon} = 1.44, C_{2\varepsilon} = 1.92, \sigma_k = 1.0, \sigma_\varepsilon = 1.3$, and the diffusion coefficients are $\Gamma_k = \mu + \frac{\mu_t}{\sigma_k}, \Gamma_\varepsilon = \mu + \frac{\mu_t}{\sigma_\varepsilon}$.

Taking the structural model with spiral blades at both the air and gas inlets as an example, the designed physical model is shown in Figure 2, with the mixing zone length designed to be 2 m. The geometric dimensions of the model were as follows: total length was about 2325 mm, air inlet diameter was 190 mm, gas inlet diameter was 250 mm, and pipe wall thickness was 10 mm. And the scale was 1:1 with the actual model. The air and gas inlets used mass flow boundary conditions, and the gas outlet used an outflow boundary condition. The gas inlet mass flow rate was 1.973968 kg/s, with an air volume fraction of 0.943; the air flow rate was 0.465045 kg/s, with an air volume fraction of 1. The numerical values reflect solver output precision and are not intended to represent experimentally measurable accuracy. By verifying the mass flow rate in the simulation results, it was found that the maximum error of the experimental conditions was 1.11×10^{-15}, and can be ignored. The concentration and flow rate of gas were based on the average operating conditions of a certain coal mine. Based on the gas flow conditions and reference to similar models, the following assumptions were made for the mixer flow field: (1) the flow in the mixer is steady; (2) both gas and air are ideal gases; and (3) gravity is neglected.

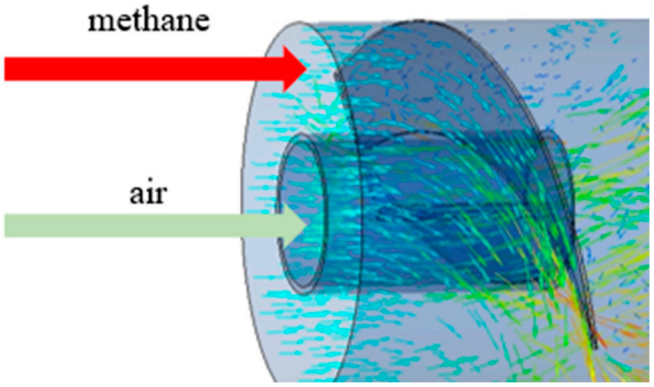


Figure 2. Schematic diagram of air flow in the device.

Steady-state RANS models assume that the flow reaches a steady state and may not fully capture the details of transient vortices, especially under conditions of high disturbance or strong turbulence. The interaction of these transient vortices may have a certain impact on the mixing performance. In addition, scale effects and uncertainty in boundary conditions in real systems are also an important factor. Our current study assumed idealized boundary conditions and ignored possible boundary effects, which may be different in actual engineering applications.

Based on these assumptions, Ansys Fluent 2023 R1 software was used for simulation, and the finite volume method was used to solve the three-dimensional N–S equations. The turbulence model used the standard $k-\varepsilon$ model. The first-order upwind scheme was used to discretize the flow equations. The wall was set as a smooth, no-slip wall condition. The convergence criteria were follows: the residuals of the continuity equation, momentum

equation, energy equation, and $k-\varepsilon$ equation decreased to at least 10^{-3}, and the flow rate at the inlet and outlet sections of the mixer was stable.

Hypermesh 2019 software was used to generate the grid for the internal flow region of the mixer. Due to the complexity of the spiral structure, a hybrid grid generation technique was employed, with unstructured grids used for the blending structure and structured grids used for the flow region in the mixing zone, and the generated computational grid is shown in Figure 3.

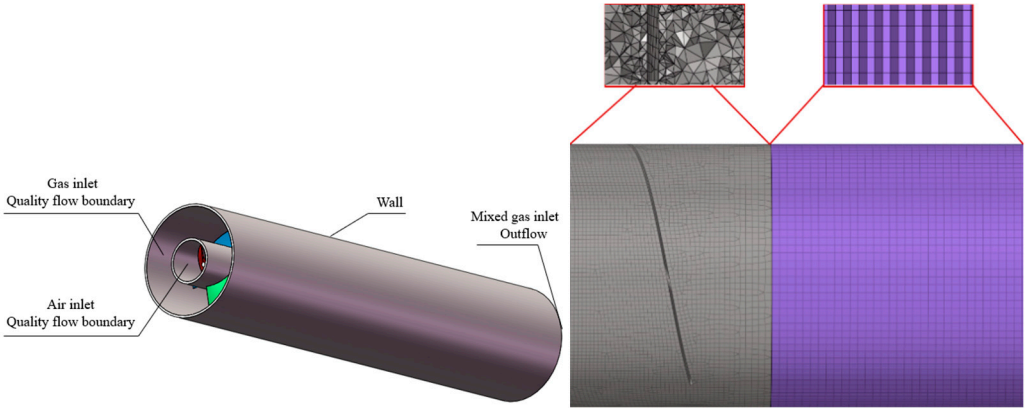


Figure 3. Physical model and grid structure diagram.

In order to verify the reliability of the numerical simulation results, this paper conducted a grid independence analysis. Five groups of models with different numbers of grids were constructed, respectively, and their simulation results under the same working conditions were compared. The spatial non-uniformity was used as an evaluation index to measure the mixing effect. As shown in Figure 4, as the total number of grids increased from about 270,000 to 870,000, the spatial non-uniformity factor decreased significantly. After exceeding 870,000 grids, the non-uniformity factor stabilized at a value of about 0.02 to 0.03. This trend shows that the simulation results were relatively insensitive to further grid refinement and showed satisfactory grid independence. The change between the last two data points was very small, and the overall convergence behavior proves that it was reasonable to use a grid of about 1.05 million grids in order to achieve a good balance between accuracy and computational efficiency. Therefore, the number of grids was determined to be about 1 million.

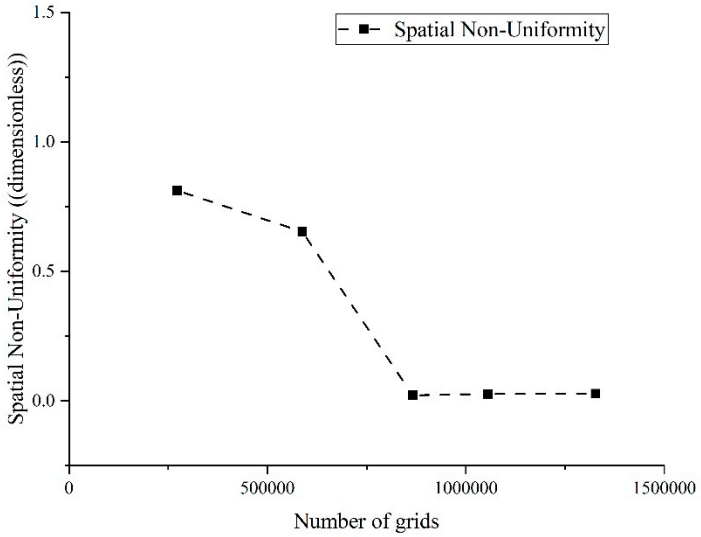


Figure 4. Grid independence verification.

4. Simulation Results Analysis

Numerical simulations were conducted for the four structures without spiral blades in the mixing zone. The streamlines of air and gas inside the mixer, as well as the methane mass fraction distribution along the YZ plane and at the outlet, are shown in Figures 5 and 6. Analysis of the images shows that when only the air inlet had a spiral blade structure, due to the small air flow rate, the rotation of air had a relatively small disturbance on the overall gas flow, which was beneficial for axial flow and reduces pressure loss. However, the relative motion between air and gas was small, resulting in poor mixing, the uneven distribution of gas at the outlet, and a tendency for gas to accumulate at the pipe edges. Under the structure where only gas rotates, the central air was effectively driven to mix, and the relative motion between air and gas was significant, resulting in better mixing and less gas accumulation at the edges, with relatively higher pressure loss compared to the structure where only air rotates. When both air and gas rotated in the same direction, the overall rotation effect was significant, but the relative motion between the two was small, which slightly reduced pressure loss, but had little effect on the mixing of air and gas, with significant gas accumulation at the pipe edges. When both air and gas rotated in opposite directions, the rotation effect was significant, and the relative motion between the two was significant, increasing the number of collisions between the two gases, which was beneficial for mixing. However, the pressure loss increased slightly. As shown in Figure 6c, the gas accumulation at the pipe walls was significantly reduced, and the overall mixing effect was excellent.

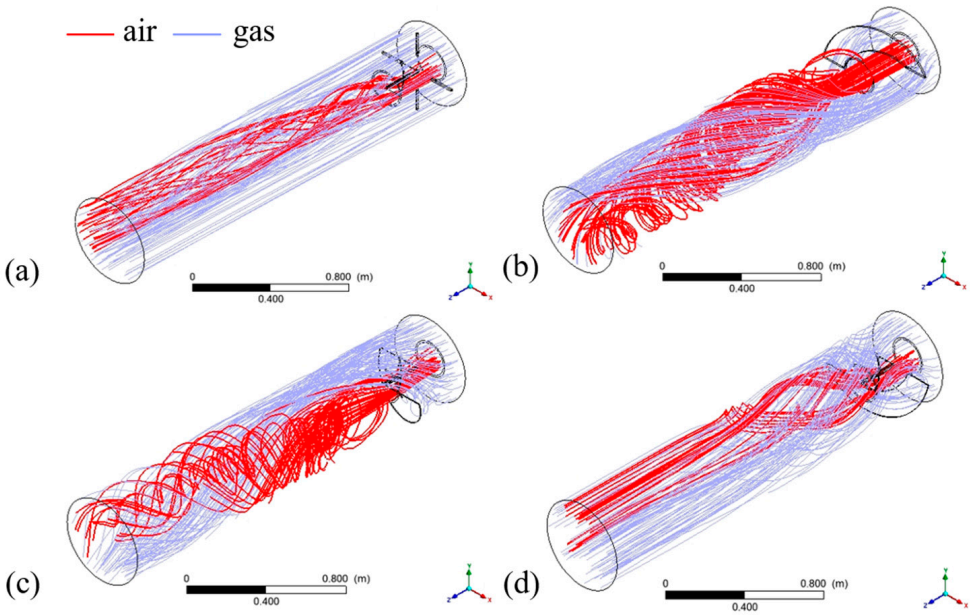


Figure 5. Streamline diagram air and gas in mixer. (**a**) Air rotation, (**b**) gas rotation, (**c**) air–gas counter-rotating, and (**d**) air–gas co-rotating.

The total pressure at various cross-sections of the four structures without spiral blades in the mixing zone was area-weighted averaged, and the total pressure variation along the cross-section is shown in Figure 7. The zero point on the horizontal axis in the figure is the outlet position of the spiral structure. As shown in Figure 7, when only air rotated, the pressure loss was the lowest, much lower than the other three structures, and the pressure loss along the cross-section area did not change much. The pressure loss trend of the structure where air and gas rotated in opposite directions was similar to that of the structure where only gas rotated, but the overall pressure loss of the structure where only gas rotated was slightly lower than that of the structure where air and gas rotated in

opposite directions, indicating that air rotation had little effect on the overall pressure loss. At 0.81 m from the outlet of the spiral structure, the pressure loss of the air and gas counter-rotating structure was higher than that of the air and gas co-rotating structure. Beyond this position, the pressure loss of the air and gas co-rotating structure was greater than that of the air and gas counter-rotating structure. According to the analysis of Figure 5c,d, this is because the co-rotating airflow near the outlet was close to stable and the pressure level gradually decreased. The flow field of the counter-rotating airflow still had a strong relative motion, which kept the pressure at a certain level, so the pressure drop was smaller than that of the co-rotating airflow. In addition, the pressure cloud diagrams of the air and gas counter-rotating structure and the air and gas co-rotating structure are shown in Figure 8. Compared with the air and gas co-rotating structure, the pressure on the outlet cross section of the air and gas counter-rotating structure was higher.

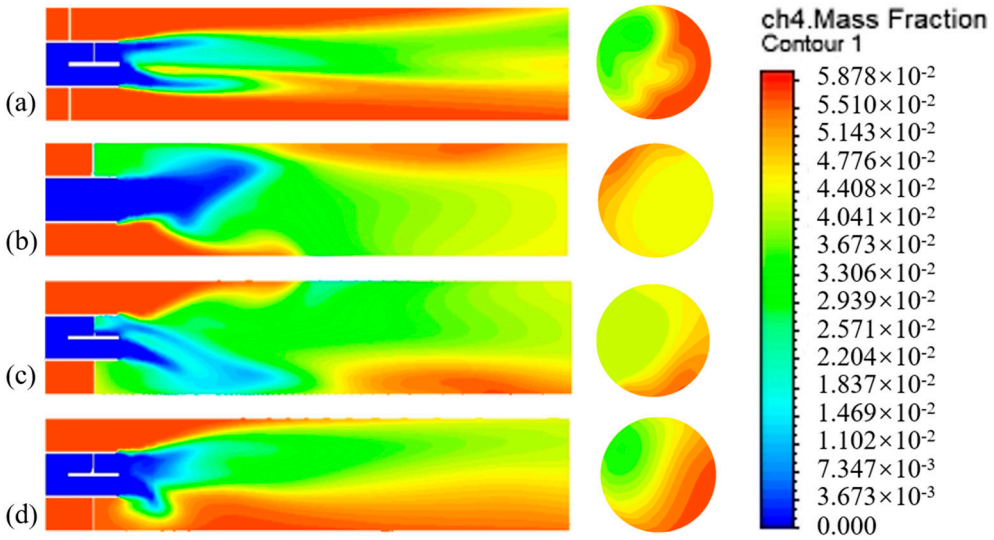


Figure 6. Gas distribution map along the mixer's axial plane and outlet surface. (**a**) Air rotation, (**b**) gas rotation, (**c**) air–gas counter-rotating, and (**d**) air–gas co-rotating.

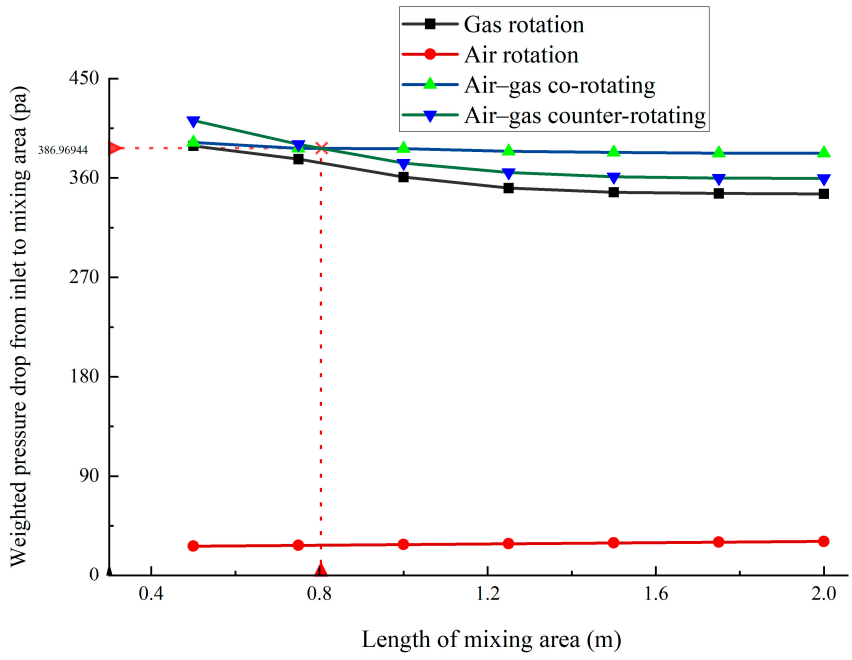


Figure 7. Variation diagram of total pressure with cross section along the mixer.

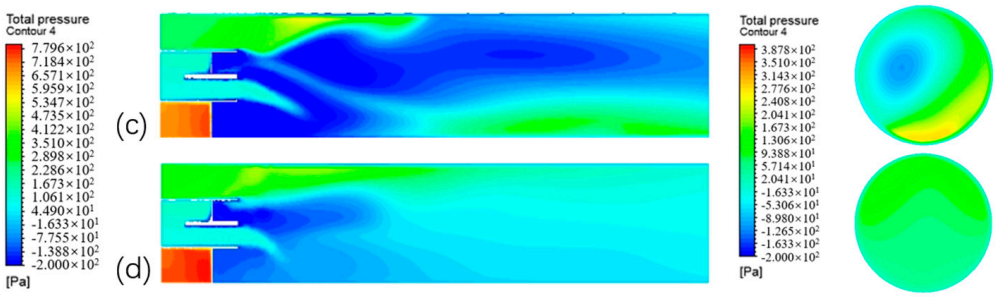


Figure 8. Pressure distribution contours along the mixer axis plane and outlet surface. (**c**) Air–gas counter-rotating. (**d**) Air–gas co-rotating.

The spatial non-uniformity of gas and air refers to the degree of non-uniformity of the gas concentration distribution on the cross-section of interest, often represented by SMD [22]. A larger SMD indicates worse mixing, while a smaller SMD indicates better mixing. There are many methods to evaluate spatial non-uniformity. In this paper, the method used by FENG Chong et al. [22] of Tsinghua University to study the mixing performance of the R0110 heavy-duty gas turbine combustor was used to evaluate the mixing performance.

$$N_s = \overline{(\sigma_f / C_f)} \tag{7}$$

$$\sigma_f = \sqrt{\frac{1}{N-1}\sum_{i=1}^{N}(C_{f,i} - \overline{C_f})^2} \tag{8}$$

where $\overline{C_f}$ represents the spatial average of the gas concentration on a certain cross-section, σ_f represents the corresponding concentration deviation, and N_s is the average spatial non-uniformity of the mixed gas and air.

Figure 9 shows the spatial non-uniformity of the gas concentration on the cross-section of the mixer under the four blending structures. As shown in the figure, as the length of the mixing zone increased, the spatial non-uniformity generally decreased, with the most significant decrease observed in the structure where only gas rotated. When the mixing zone reached a certain length, the spatial non-uniformity under the structures where only air rotated and where air and gas rotated in the same direction stabilized, and further increasing the mixing zone length did not significantly improve the gas mixing effect. When the mixing zone length was short, the structure with the same rotation direction performed relatively better, but the spatial non-uniformity was still greater than 15%. The minimum mixing zone length required to achieve a spatial non-uniformity of less than 15% was 1.1 m. Comparing the structure where only gas rotated and the structure where air and gas rotated in opposite directions, it can be seen that the air rotation had little effect on the gas mixing effect, and as the mixing zone length increased, the difference in spatial non-uniformity gradually decreased. At 2 m, the spatial non-uniformity of the structure where only gas rotated and the structure where air and gas rotated in opposite directions reached the lowest, about 8%, which meets the requirement of less than 15% spatial non-uniformity in engineering requirement.

Figure 10 shows the pressure loss at the inlet and outlet, and the spatial non-uniformity of the outlet gas for the four structures with clockwise or counterclockwise spiral blades added at the forefront of the mixing zone. The structure numbers are shown in Table 1. As shown in the figure, the a1 and a2 structures had similar effects. Compared to the a structure, the spatial non-uniformity of the outlet gas decreased by 60%, but the pressure loss increased significantly, from 30.8 Pa to 200–300 Pa. The b1 structure had the best gas mixing effect among all the structures with helical blades at the front end of the mixing

zone, but its pressure loss far exceeded that of the other structures. According to the data, the b2 structure had a slightly higher pressure loss than the b structure, and the outlet spatial non-uniformity was slightly lower. The c1 structure had a 67.7% decrease in outlet non-uniformity compared to the c structure, while the c2 structure had a 54.4% decrease, but the pressure loss of the c1 structure increased from 359 Pa to 1135 Pa, and the c2 structure increased from 359 Pa to 605 Pa. The d1 structure had the worst mixing effect, and its pressure loss was also at a high level. The d2 structure had an 84% decrease in outlet non-uniformity compared to the d structure, but its pressure loss was still at a high level.

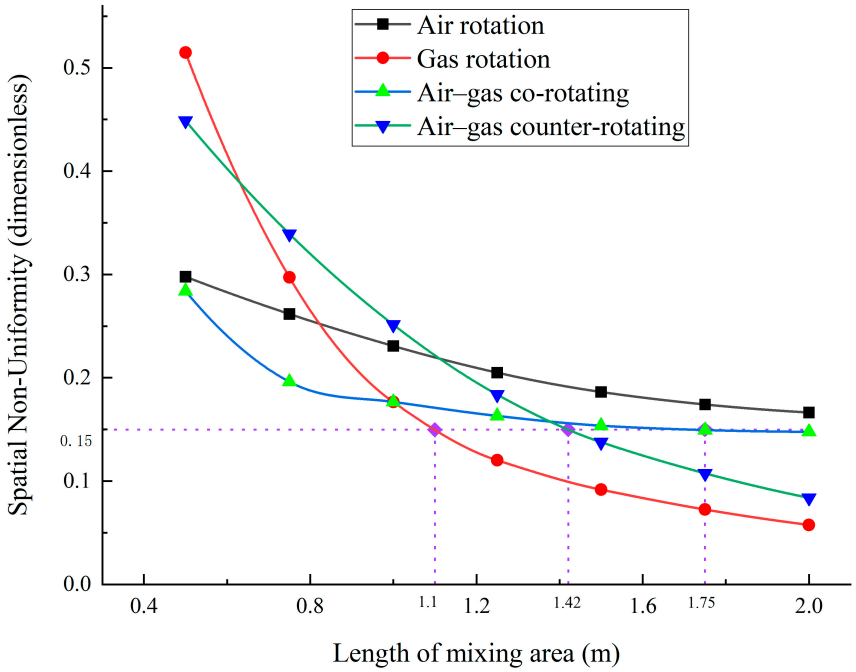


Figure 9. Diagram of spatial non-uniformity variation along the cross section of the mixer.

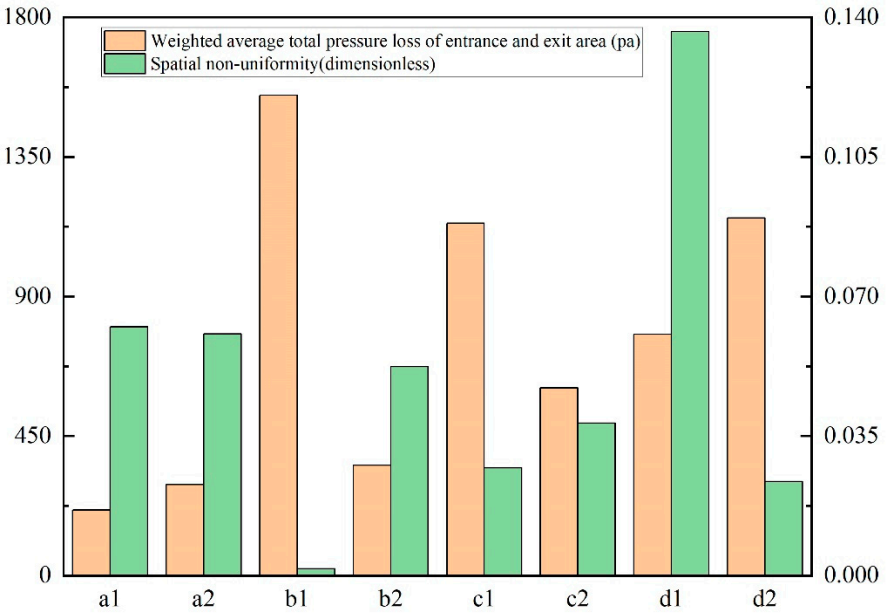


Figure 10. Pressure loss at inlet and outlet and non-uniformity of outlet gas space.

Table 2 shows the spatial non-uniformity data of the gas at different cross-sections in the eight different mixer structures with spiral blades added at the forefront of the mixing zone. As shown in the table, the spatial non-uniformity decreased as the length increased,

with the a1 structure showing a decrease of up to 0.3061, far exceeding the other structures. Comparing the cross-sectional data at 0.5 m, the b1 structure had a spatial non-uniformity as low as 3.5%, with an improvement of more than 10% compared to the other structures. When the length reached 1.25 m, the spatial non-uniformity of all structures decreased to less than 15%, showing a significant improvement in performance compared to the mixer structures without helical blades at the front end of the mixing zone.

Table 2. Non uniformity of cross-sectional space at different positions.

Model \ Length	0.5 m	0.75 m	1 m	1.25 m	1.5 m	1.75 m	2 m
a1	0.36846	0.28228	0.19744	0.14179	0.10695	0.08219	0.06236
a2	0.32407	0.23786	0.16193	0.12253	0.09562	0.07371	0.06057
b1	0.03589	0.02269	0.01741	0.01111	0.00650	0.00352	0.00170
b2	0.31912	0.20955	0.13853	0.10213	0.08070	0.06508	0.05237
c1	0.22191	0.14100	0.10767	0.08387	0.06398	0.04829	0.02696
c2	0.19589	0.10601	0.06668	0.05474	0.04886	0.04247	0.03823
d1	0.33088	0.23683	0.19968	0.17827	0.16091	0.14767	0.13642
d2	0.12011	0.09312	0.07193	0.05260	0.03910	0.03032	0.02353

5. Conclusions

Based on the above results, the following conclusions can be drawn:

1. Installing spiral blades at the gas inlet significantly improves the overall mixing effect compared to installing them at the air inlet.
2. When spiral blades are installed at both the air and gas inlets, the direction of rotation of the blades has an impact: when the mixing zone is short, the pressure loss and spatial non-uniformity are relatively lower for the same rotation direction, but when the mixing zone is long, the opposite rotation direction has a greater advantage.
3. When no spiral blades are added to the front end of the mixing zone, the overall effect of the structure with only gas rotation is the best, and the effect of the structure with air and gas rotating in opposite directions is similar to that of the structure with only gas rotation at two meters in the mixing zone.
4. Adding spiral blades at the forefront of the mixing zone significantly improves gas uniformity but is not conducive to reducing pressure loss. The impact on pressure loss and gas uniformity is related to the direction of rotation. Adding a set of spiral blades with the opposite rotation direction to the blades at the low-concentration gas inlet at the forefront of the mixing zone can greatly improve the mixing uniformity at the outlet but will increase the system's mixing pressure loss. When the two rotation directions are the same, the impact on system pressure loss and mixing uniformity is relatively small.
5. Among the structures with spiral blades added at the forefront of the mixing zone, the b2 structure has the most ideal results, with an outlet spatial inhomogeneity of approximately 5.24%, significantly better than the requirement of less than 15% spatial non-uniformity in the "Design Code for Low-Concentration Gas Oxidation and Utilization Engineering in Coal Mines", and the spatial non-uniformity still tends to decrease as the mixing zone length increases.

In summary, the proposed spiral blade configurations effectively enhanced mixing uniformity while balancing pressure loss. However, this study is based solely on numerical simulations. The lack of experimental validation is a limitation, and future studies will focus on laboratory or field experiments to further verify the findings.

Author Contributions: Conceptualization, Q.H.; Methodology, H.G.; Software, X.G. and S.L.; Validation, Y.L.; Formal analysis, H.G.; Investigation, H.G.; Resources, X.G.; Data curation, H.G. and S.L.; Writing—original draft, H.G. and S.L.; Writing—review & editing, Y.L.; Visualization, Q.H.; Project administration, Y.L.; Funding acquisition, X.G., Q.H. and Y.L. All authors have read and agreed to the published version of the manuscript.

Funding: This work was financially supported by the National Key Research and Development Program of China (Project NO. 2023YFF0615404).

Institutional Review Board Statement: Not applicable.

Informed Consent Statement: Not applicable.

Data Availability Statement: The original contributions presented in the study are included in the article, further inquiries can be directed to the corresponding author.

Acknowledgments: The authors are grateful to the anonymous reviewers for their extraordinary advice.

Conflicts of Interest: Authors Han Gao and Xuanping Gong were employed by the company Middling Coal Energy Research Institute Co., Ltd. The remaining authors declare that the research was conducted in the absence of any commercial or financial relationships that could be construed as a potential conflict of interest.

References

1. Gajdzik, B.; Tobór-Osadnik, K.; Wolniak, R.; Grebski, W.W. European Climate Policy in the Context of the Problem of Methane Emissions from Coal Mines in Poland. *Energies* **2024**, *17*, 2396. [CrossRef]
2. Chai, X.; Tonjes, D.J.; Mahajan, D. Methane emissions as energy reservoir: Context, scope, causes and mitigation strategies. *Prog. Energy Combust. Sci.* **2016**, *56*, 33–70. [CrossRef]
3. Bibler, C.J.; Marshall, J.S.; Pilcher, R.C. Status of worldwide coal mine methane emissions and use. *Int. J. Coal Geol.* **1998**, *35*, 283–310. [CrossRef]
4. Chandrsuda, C.; Mehta, R.D.; Weir, A.D.; Bradshaw, P. Effect of free-stream turbulence on large structure in turbulent mixing layers. *J. Fluid. Mech.* **1978**, *85*, 693–704. [CrossRef]
5. Ottino, J.M. Mixing, chaotic advection, and turbulence. *Annu. Rev. Fluid. Mech.* **1990**, *22*, 207–254. [CrossRef]
6. Gu, W.; Liu, X.; Wang, Z.; Zheng, H. Applications of PLIF in fundamental research on turbulent combustion of hydrogen and hydrogen hybrid fuels: A brief review. *Int. J. Hydrogen Energy* **2024**, *78*, 1240–1274. [CrossRef]
7. Sun, J.; Wang, J.; Li, Z. Tuning of Mixing Zone Parameters in a Dynamic Mixer and Performance Comparison with Screw-Based Mixers. *Mechanics* **2023**, *29*, 309–316. [CrossRef]
8. Meijer, H.E.; Singh, M.K.; Anderson, P.D. On the performance of static mixers: A quantitative comparison. *Prog. Polym. Sci.* **2012**, *37*, 1333–1349. [CrossRef]
9. Mahajan, D.; Tan, K.; Venkatesh, T.; Kileti, P.; Clayton, C.R. Hydrogen blending in gas pipeline networks—A review. *Energies* **2022**, *15*, 3582. [CrossRef]
10. Sharma, S.; Sahir, A.H. Natural Gas and hydrogen blending: A perspective on numerical modeling and CFD analysis for transient and steady-state scenarios. *Chem. Prod. Process Model.* **2025**, *20*, 129–158. [CrossRef]
11. El-Mahallawy, F.; Abdelhafez, A.; Mansour, M.S. Mixing and nozzle geometry effects on flame structure and stability. *Combust. Sci. Technol.* **2007**, *179*, 249–263. [CrossRef]
12. Xiao, Q.; Tsai, H.M.; Papamoschou, D.; Johnson, A. Experimental and numerical study of jet mixing from a shock-containing nozzle. *J. Propuls. Power* **2009**, *25*, 688–696. [CrossRef]
13. Zhang, J.X. Analysis on the effect of venturi tube structural parameters on fluid flow. *AIP Adv.* **2017**, *7*, 065315. [CrossRef]
14. Zheng, J.; Xu, W.; Jia, G.; Shi, Y.; Cai, M. Performance analysis of coaxial shear static mixer for hydrogen blending into natural gas. *Int. J. Hydrogen Energy* **2024**, *78*, 1275–1287. [CrossRef]
15. Li, F.; Dong, S.; Chen, L.; Zhu, X.; Han, Z. Key safety technologies and advances in long-distance pipeline transportation of hydrogen blended natural gas. *Mech. Eng.* **2023**, *45*, 230–244.
16. Zhang, C.; Ferrell, A.R.; Nandakumar, K. Study of a toroidal-helical pipe as an innovative static mixer in laminar flows. *Chem. Eng. J.* **2019**, *359*, 446–458. [CrossRef]
17. Rabha, S.; Schubert, M.; Grugel, F.; Banowski, M.; Hampel, U. Visualization and quantitative analysis of dispersive mixing by a helical static mixer in upward co-current gas–liquid flow. *Chem. Eng. J.* **2015**, *262*, 527–540. [CrossRef]

18. Su, Y.; Li, J.F.; Yu, B.; Zhao, Y.L.; Han, D.X.; Li, J.L. Simulation study on the mixing of hydrogen and natural gas in static mixers. *Nat. Gas. Ind.* **2023**, *43*, 113–122.
19. Qiao, Y.; Zheng, L.; Guo, K.; Liu, H.; Zhang, B.; Li, W.; Guo, X.; Liu, C. Numerical study of flow field and mixing performance of a new curved-sheet blade-folded static mixer. *Ind. Eng. Chem. Res.* **2024**, *63*, 7836–7852. [CrossRef]
20. Zhang, Q. Low concentration gas metal fiber combustion technology and its experimental study. *Coal Chem. Ind.* **2024**, *52*, 120–123.
21. Savicki, D.L.; Goulart, A.; Becker, G.Z. A simplified k-ϵ turbulence model. *J. Braz. Soc. Mech. Sci. Eng.* **2021**, *43*, 384. [CrossRef]
22. Feng, C.; Qi, H.Y.; Xie, G.; Chen, X. Analysis on the issue of fuel/air premixing uniformity of the dry low NOx gas turbine combustor. *Proc. CSEE* **2011**, *31*, 9–19.

Disclaimer/Publisher's Note: The statements, opinions and data contained in all publications are solely those of the individual author(s) and contributor(s) and not of MDPI and/or the editor(s). MDPI and/or the editor(s) disclaim responsibility for any injury to people or property resulting from any ideas, methods, instructions or products referred to in the content.